DOI: 10.21062/mft.2022.034 © 2022 Manufacturing Technology. All rights reserved. http://www.journalmt.com

Analysis of the Effect of Preset Surface Texture on Hard State Cutting

Changlong Zhao (0000-0001-7778-3494), Chen Ma (0000-0002-4884-235X), Zhenrong Ma (0000-0001-6300-2300), Junbao Yang (0000-0002-4958-6546), Ming Li (0000-0003-4202-0256)
College of mechanical and vehicle engineering, Changchun University, Changchun 130022.Changlong Zhao, China. E-mail: zhao19790204@126.com; 2628897767@qq.com.

When cubic boron nitride (CBN) tools are used for hard cutting hardened steel, a large cutting force is generated. This is accompanied by a large amount of cutting heat, resulting in serious tool wear. In this study, we combined surface weaving technology with hard cutting. Design simulations and experiments were performed on three-factor untextured orthogonal cutting by considering parameters such as depth of cut, cutting speed, and feed. Subsequently, the simulation and experimental data were analyzed by using the polar difference, variance, and signal-to-noise ratio methods to determine the best combination of cutting parameters and the degree of influence of each parameter on the cutting force generated during hard cutting. Hardened GCr15 steel with preset surface texture was hard cut using the optimal combination of cutting parameters. Consequently, tool wear was observed, and the cutting forces were measured. The results were compared with those obtained from the equivalent cutting conditions without texture. The results revealed that a minimum cutting force of 71.48 N was obtained in the untextured cutting experiment. Additionally, a minimum cutting force of 44.64 N was measured in the preset surface texture cutting experiment under the same conditions, which was approximately 37.55% lower than the result obtained in the untextured cutting experiment. The tool wear was much higher for untextured cutting than for preset surface texture cutting. The comparative experiments performed, with and without texture, indicated that a combination of surface texture technology and hard cutting can effectively reduce the cutting forces and tool wear and improve tool life.

Keywords: Hardened steel; Hard cutting; Orthogonal experiments; Cutting force; Preset texture; Tool wear

1 Introduction

Due to its high strength and wear resistance, hardened steel is mainly used in bearings, molds, automotive and other fields. However, the material is difficult to process [1-3]. The hardness of quench hardened steel can reach 520–840 HV. When hardened steel is subjected to normal cutting, the cutting force between the tool and the workpiece is large, and the cutting heat cannot be discharged in time. This increases the cutting temperature of the tool, aggravating tool wear and reducing tool life. Thus, there is an urgent need for an economic and efficient method for machining hardened steel. Ales Jaros et al [4] added a PVD or CVD coating to the surface of the milling cutter and succeeded in reducing the force loading on the tool, which in turn reduced the wear on the back tool face and extended the tool life. Sigit Yoewono Martowibowo et al [5] selected tool tip radius, cutting speed, feed rate and depth of cut as the most important process parameters and successfully optimized the optimal process parameters for turning using genetic algorithm. Tippana Sahachar Reddy et al [6] used a carbide tool for hardened H13 steel to verify the relationship between the depth of cut, cutting speed, and feed on the cutting forces. Y.Kevin Chou et al [7] used a cubic boron nitride tool for hard cutting AISI5 to improve the surface roughness by reducing the depth of cut. János Kundrák et al [8] proposed a tool life function, which is applicable to the entire speed range. The results of the study showed that at speeds below the tool life maximum, wear and staining lead to tool degradation, while at speeds above this, thermally activated degradation processes play an increasing role with plays an increasing role as the speed increases. Denis Boing et al [9] used coated carbide, hybrid ceramic, and polycrystalline cubic boron nitride tools for hard cutting AISI52100 steel to verify the effect of tool wear at different cutting speeds. The authors found that the polycrystalline cubic boron nitride tools showed the lowest wear rate at the cutting speed of 120 m/min. Meanwhile, the coated carbide tools exhibited the lowest wear rate at the cutting speed of 150 m/min. The lowest wear rate was observed at the cutting speed of 120 m/min for polycrystalline cubic boron nitride tools, 150 m/min for coated tungsten carbide tools, and 187.5 m/min for hybrid ceramic tools. Hard cutting tools currently give rise to problems, such as generating large cutting forces and causing serious tool wear, during hard-state cutting. Therefore, productive machining methods and auxiliary cutting methods are emerged. Productive machining methods

include adjustment of cutting parameters and optimization of tool trajectory [10], and auxiliary cutting methods include laser heating-assisted cutting and ultrasonic vibration-assisted cutting [11-15]. They combine traditional cutting technology and auxiliary processing technology to reduce tool cutting forces and thus improve tool life. However, such new auxiliary processing methods are expensive and come with some drawbacks. When examining the progress of ultrasonic vibration-assisted cutting of composite materials, Zhou Bojian et al [16] stated that although the method reduces the cutting force compared with the traditional cutting method, there is no perfect method for the control and solution of edge defects or burrs and surface defects during the cutting process. In addition, Zhanwei Bo [17] mentioned that during laser-assisted cutting, when the laser parameters and cutting dosage are correctly selected, the cutting force and tool wear can be reduced. However, the method is expensive and requires a reasonable placement of the laser on the machine tool.

In this study, we combined hard-state cutting with electrical discharge machining (EDM) perforation technology. We used this technology to preset the surface texture of the workpiece. Hard-state cutting was then performed on the workpiece, and a controlled cutting experiment with preset texture and no texture was conducted to verify the effectiveness of preset texture on the workpiece surface. The results revealed that the proposed technique can reduce the cutting force and tool wear and increase tool life.

2 Simulation and analysis of cutting of non-texture GCr15 hardened steel

2.1 Simulation model and material selection

In this study, hardened GCr15 bearing steel was selected as the workpiece material for cutting simulation. It has a high and uniform hardness, good wear resistance, and high fatigue strength [18-21]. The dimensions of the workpiece chosen for cutting simulation were as follows: diameter D=10mm and height H=5mm.

The characteristic properties of hardened GCr15 bearing steel are shown in Tab. 1. The Johnson–Cook intrinsic relationships and parameters [22] are shown in Tab. 2.

Tab. 1 *Characteristic performance of GCr15 bearing steel*

Performance	Density/kg/m³	Melting point/℃	Poisson's ratio	Young's modulus/GPa	Coefficient of thermal expansion/10^{-6}/℃
GCr15	7827	1487	0.277	210	11.9

Tab. 2 *GCr15 bearing steel material Johnson Cook constitutive relationship and parameter table*

A(MPa)	B/MPa	n	c	M
688.17	150.82	0.3362	0.0428	2.7786

In Tab. 2, A is the initial yield stress, B is the strain hardening modulus, n is the strain hardening index, c is the strain rate strengthening parameter, and m is the thermal softening index.

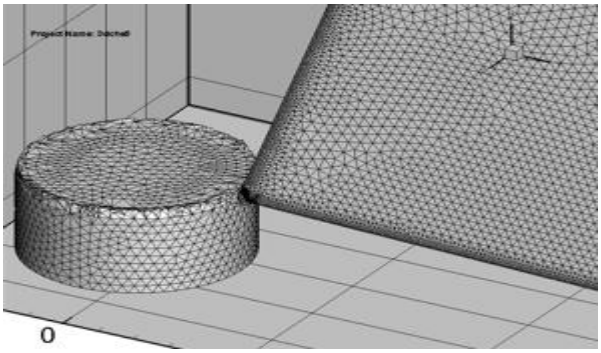

Fig. 1 *Model meshing and contact setting*

In the cutting simulation, CBN was chosen as the tool material, whose shape was set as a square. The transverse front angle was 5°, and the longitudinal front angle was 6°. The edge inclination angle was 6°, and the back angle was 5°. A 3D external cutting simulation was carried out. The mesh division is shown in Fig. 1.

2.2 Orthogonal cutting simulation and scheme of the experimental design

The factor levels of the orthogonal cutting experiment are outlined in Table 3, where the depth of cut (ap), cutting speed (v), and feed rate (f) are the experimental factors. Each experimental factor contained four levels, with a total of 16 experimental groups.

Tab. 3 *Orthogonal cutting experiment factor level table*

Symbol	Cutting parameters	level 1	level 2	level 3	level 4
v	Cutting speed（mm/min）	8500	9400	11900	15100
f	Feed amount（μm/r）	50	100	150	200
ap	Cutting depth（μm）	100	200	300	400

2.3 Signal-to-noise analysis method

The signal-to-noise ratio is the ratio of signal to noise in the system. The larger the signal-to-noise ratio, the stronger the signal [23]. The S/N ratio is calculated as follows [24]:

$$S/N(\eta) = -10\,lg\left(\frac{1}{j}\sum_{j=1}^{n} F_j{}^2\right) \qquad (1)$$

Where:
F…Cutting force,
j…Number of experiments.

2.4 Simulation results and analysis

Based on the orthogonal experimental scheme, the cutting simulation yielded the cutting force data and signal-to-noise ratio values, which are shown in Tab. 4.

Tab. 4 *Simulation cutting force data and signal-to-noise ratio*

No.	Cutting depth /μm	Cutting speed /mm/min	Feed amount /μm/r	Fr /N	S/N
1	100	8500	50	225.17	-47.05
2	200	8500	100	98.90	-39.90
3	300	8500	150	149.12	-43.47
4	400	8500	200	894.09	-59.03
5	200	9400	50	327.45	-50.30
6	300	9400	100	139.28	-42.88
7	400	9400	150	898.61	-59.07
8	100	9400	200	412.31	-52.30
9	300	11900	50	215.71	-46.68
10	400	11900	100	812.40	-58.20
11	100	11900	150	492.44	-53.85
12	200	11900	200	692.82	-56.81
13	400	15100	50	482.49	-53.67
14	100	15100	100	126.59	-42.05
15	200	15100	150	428.28	-52.63
16	300	15100	200	608.79	-55.69

Where:
Fr…Cutting force data,
S/N…Signal-to-noise ratio value corresponding to each group of the experimental cutting force data.

If we observe the data presented in Table 4, in the orthogonal experimental scheme, a maximum cutting force of 898.61 N and a signal-to-noise ratio of -59.07 were obtained for the 7th group of the experimental schemes, with the following hard-cutting conditions: ap=400 μm, v=9400 mm/min, and f= 150μm/r. Alternatively, a minimum cutting force of 98.90 N and a signal-to-noise ratio of -39.90 were obtained for the 2nd group of the experimental schemes, yielding ap= 200 μm, v=8500 mm/min, and f=100 μm/r— the best combination of cutting parameters.

The signal-to-noise ratio was analyzed by the polar difference analysis method [25], and the polar difference was obtained by calculating the K_{ji} value. The polar difference analysis table is shown in Tab. 5.

Tab. 5 *Range analysis table*

Cutting parameters	Cutting depth（A）	Cutting speed（B）	Feed amount（C）
Kj1	-195.25	-189.45	-197.70
Kj2	-199.64	-204.55	-183.03
Kj3	-188.72	-215.54	-209.02
Kj4	-229.97	-204.04	-223.83
Excellent level	A3	B1	C2
Rj	41.25	26.09	40.8
Primary and secondary order		A＞C＞B	

From Tab. 4 and Tab. 5, it can be concluded that under the depth of cut factor, -229.97 and -188.72 were the maximum and minimum values of S/N ratio, respectively, R_j was 41.25, the optimal level was A3, and ap=300 μm. Additionally, under the cutting speed factor, -215.54 and -189.45 were the maximum and minimum values of S/N ratio, respectively, R_j was 26.09, the optimal level was B1, and v=8500 mm/min. Under the feed factor, -223.83 and -183.03 were the maximum and minimum values of S/N ratio, respectively, R_j was 40.8, the optimal level was C2, and f=100 μm/r. The relationship between the degree of influence of the three factors on the cutting force during hard cutting can be given by $v < f < ap$.

The cutting force at each moment of the second set of cutting simulation was derived to obtain the cutting force curve, as shown in Fig. 2. The curve was fitted to the initial cutting force curve, and the results are shown in Fig. 3. For the second set of hard-cutting simulation, the data processing of the second set of simulated cutting force data resulted in an average cutting force of 83.67 N.

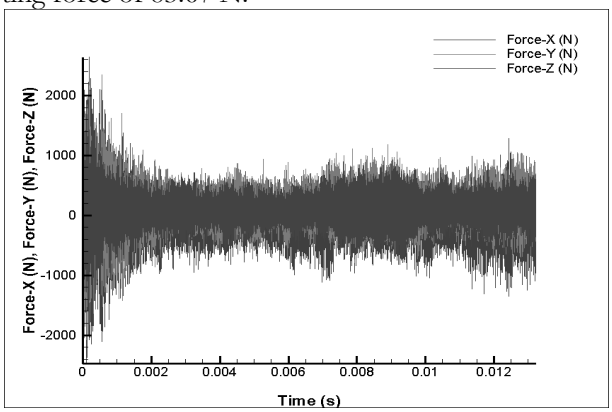

Fig. 2 *Cutting force curve*

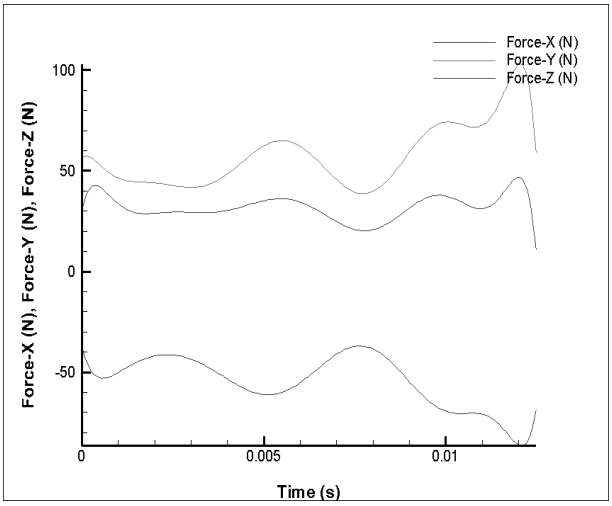

Fig. 3 *Cutting force fitting curve*

The cutting force data obtained from the cutting simulation were processed by the ANOVA method [26]. Tab. 6 shows the results obtained from ANOVA after processing. After selecting the appropriate α value, comparing the F distribution table, finding out the F_α value, and comparing the size of F and F_α values after ANOVA processing, if $F>F\_\alpha$, it means that the factor is significant at the significance level α, and vice versa, it is not significant. When α=0.05 and F_α=4.76, from Tab. 6, it can be observed that $F_V<F_{0.05}<F_f<F_{ap}$. It can thus be concluded that the three factors on the relationship between the degree of influence of the three factors on the cutting force: v < f < ap. In addition, the relationship between the magnitude of contribution of the three factors on the influence of cutting force can be given by v (13.92%) < f (36.31%) < ap (40.59%).

Tab. 6 *Simulation table of cutting force data and signal-to-noise ratio analysis*

Cutting parameters	Degree of freedom	Self-differential sum of squares	Mean Square	F	Speciality	Contribution rate (%)
Cutting depth	3	250.507	83.502	8.852	0.013	40.59
Cutting speed	3	85.929	28.643	3.036	0.115	13.92
Feed rate	3	224.099	74.700	7.919	0.017	36.31
Error	6	56.599	9.433			9.17
Total	15	617.133				

3 Design and analysis of non-texture cutting experiments

The orthogonal cutting experimental scheme [27-28] was set up in the same way as the simulation scheme. The specific parameters are outlined in Tab. 1.

3.1 Orthogonal cutting experiment of non-texture Gcr15 hardened steel

3.1.1 Experimental equipment

Fig. 4 *Cutting force acquisition device diagram*

The cutting experiment employed the cutting force measurement system comprising the Swiss Kistler data collector 5697A, Kistler 5070A10000 multi-channel charge amplifier, Kistler multicomponent force meter 9257B, and a computer-aided system. Fig. 4 depicts the physical diagram of the cutting force acquisition system.

3.1.2 Experimental workpieces and tools

The hardened cutting workpiece was hardened GCr15 bearing steel (0.6×2 cm). Before starting the experiment, the workpiece was heat-treated and its hardness was measured using a microhardness tester, which showed values ranging from 660–760 HV. The experimental tool was a CBN tool with CNMG120408 insert of grade YBC25 and shank model MCLNR2525M12.

3.2 Analysis of cutting experiment results

Tab. 7 shows the cutting force data and S/N ratio values obtained from the cutting experiments. From Tab. 7, in the orthogonal cutting experiments, it can be seen that the maximum cutting force of 1089.66 N was obtained in the 7th group of hard-state cutting experiments, with the S/N ratio of -60.75. The cutting conditions were as follows: ap=400 μm, v=9400 mm/min, and f=150 μm/r. The minimum cutting force of 84.26 N was obtained in the 2nd group of hard-state cutting experiments, with the S/N ratio of -38.51 and cutting conditions of ap= 200 μm, v=8500 mm/min, and f=100 μm/r.

Tab. 7 *Cutting force data and signal-to-noise ratio analysis table*

No.	Cutting depth/μm	Cutting speed/m/min	Feed amount/μm/r	F1 /N	S/N
1	100	8500	50	258.43	-48.25
2	200	8500	100	84.26	-38.51
3	300	8500	150	176.85	-44.95
4	400	8500	200	859.43	-58.68
5	200	9400	50	358.40	-51.09
6	300	9400	100	153.94	-43.75
7	400	9400	150	1089.66	-60.75
8	100	9400	200	366.99	-51.29
9	300	11900	50	226.75	-47.11
10	400	11900	100	894.33	-59.03
11	100	11900	150	410.59	-52.27
12	200	11900	200	685.38	-56.72
13	400	15100	50	458.57	-53.23
14	100	15100	100	134.06	-42.55
15	200	15100	150	484.84	-53.71
16	300	15100	200	651.54	-56.28

The cutting force data obtained from the hard-cutting experiments were analyzed using the extreme difference analysis method. Using this method, the cutting force data was obtained, which is shown in Tab. 8. As can be seen from Tab. 8, the maximum S/N ratio value under the cutting depth factor was -231.692. The minimum was -192.088 and Rj was 39.684, i.e., the optimal level was A3, ap=300 μm. The maximum S/N ratio value under the cutting speed factor was -215.128. The minimum was -190.338 and Rj was 24.790, i.e., the optimal level was B1, v= 8500 mm/min. The maximum S/N value under the feed factor was -222.972. The minimum was -183.840 and Rj was 39.132, i.e., the optimal level was C2, f=100 μm/r.

From the above analysis, it can be seen that the second group of hard-state cutting experiments, ap=300 μm, v=8500 mm/min, and f=100 μm/r, gave rise to the best combination of cutting parameters. The cutting force curve is shown in Fig. 5. It was obtained by using the Kistler force measuring instrument under the optimal combination of cutting parameters. The data of the second group of cutting force experiments were also processed. The average value of cutting force of the second group of hard-state cutting experiments was 71.48 N. In summary, the degree of influence on the cutting force can be depicted as follows: $v < f < ap$.

Tab. 8 *Range analysis table of cutting force data*

Cutting parameters	Cutting depth（A）	Cutting speed（B）	Feed amount（C）
Kj1	-194.360	-190.338	-199.680
Kj2	-200.028	-206.880	-183.840
Kj3	-192.088	-215.128	-211.680
Kj4	-231.692	-205.772	-222.972
Excellent level	A3	B1	C2
Rj	39.684	24.790	39.132
Primary and secondary order		A＞C＞B	

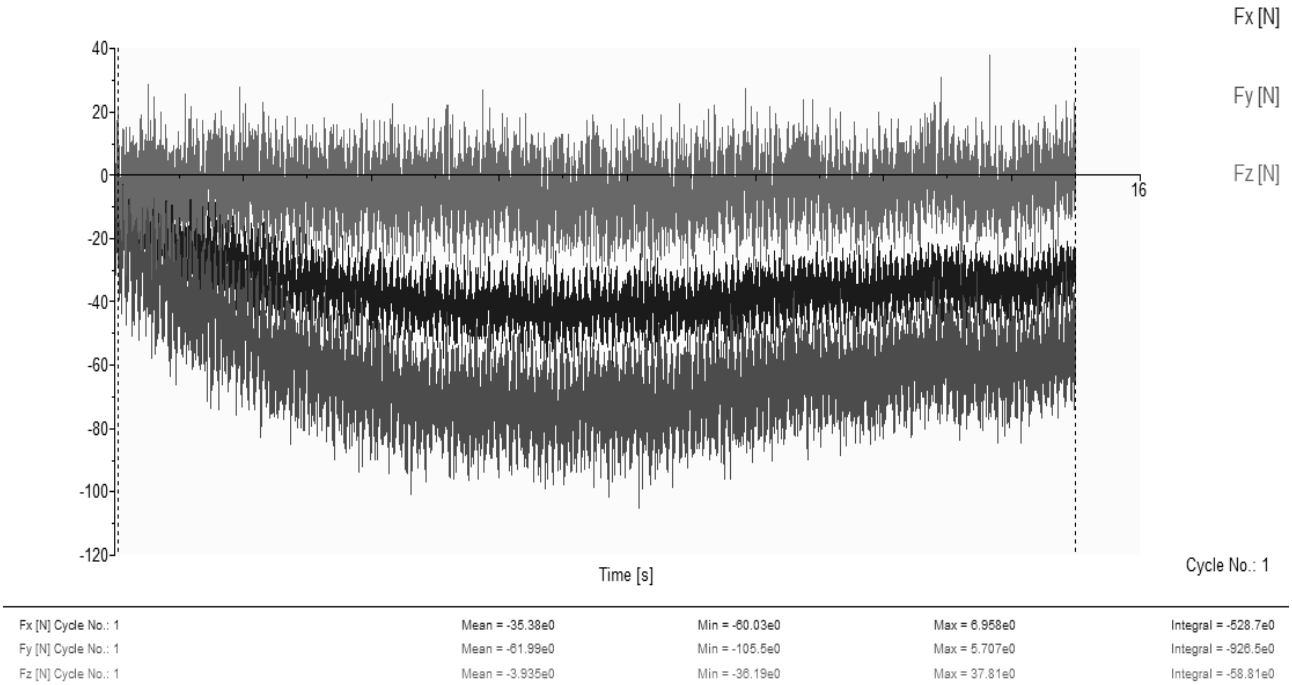

（ap=300μm、v=8500mm/min、f=100μm/r）

Fig. 5 *Experimental cutting force curve*

Tab. 9 *Cutting force data and signal-to-noise ratio analysis table*

Cutting parameters	Degree of freedom	Self-differential sum of squares	Mean Square	F	Speciality	Contribution rate (%)
Cutting depth	3	79.840	26.61	1.82	0.24	12.63
Cutting speed	3	210.68	70.23	4.81	0.05	33.33
Feed rate	3	254.02	84.67	5.80	0.03	40.19
Error	6	87.56	14.59			13.85
Total	15	632.10				

When the simulated and experimental data were compared, there were small errors between them. However, the results tended to be consistent, further verifying the feasibility of simulation for parameter optimization.

4 Preset surface texture processing experiment

EDM [29] was used in the experiments to process the surface texture and the parameters pertaining to the experimental apparatus, which are shown in Tab. 10.

Tab. 10 *EDM test instrument parameters*

Equipment name	CTD high-speed small hole processing machine
Production company	Beijing Dumont Carter Machine Co.,Ltd
Working fluid	Distilled water
Electrodes	Molybdenum wire
Electrode radius	200μm
Discharge channel radius	200μm
Voltage	15V
Current	10A
Pulse width	3ms

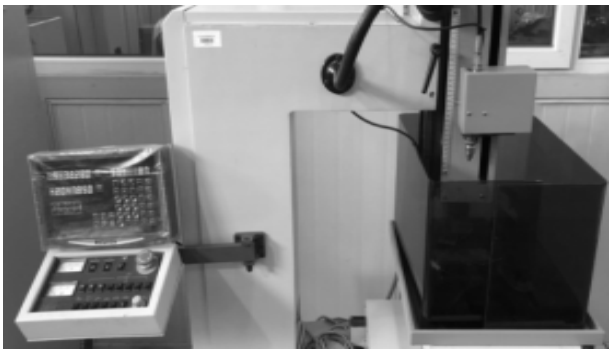

Fig. 6 *EDM scene*

Fig. 7 *Pit texture measurement scene*

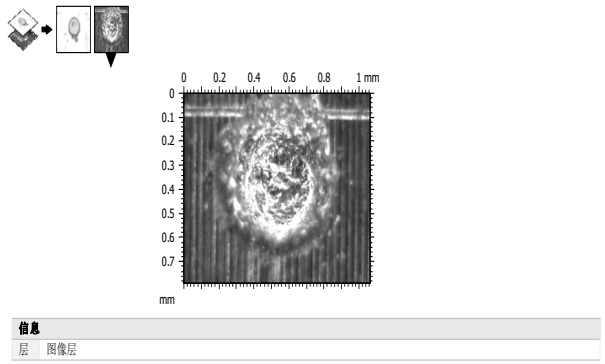

Fig. 8 *Single pit texture image layer*

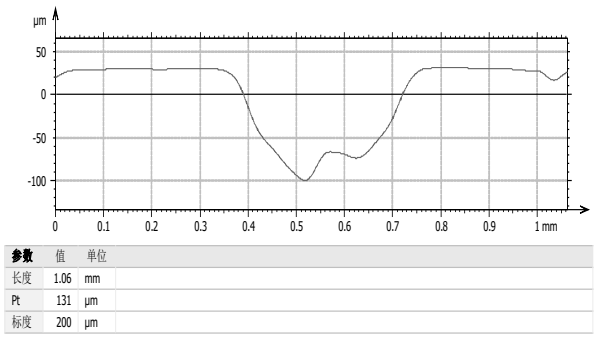

Fig. 9 *Depth diameter curve of pit texture*

The EDM object was GCr15 hardened bearing steel (0.6×2 cm) with a 30° circumferential angle between the textures and 5 mm axial spacing. Fig. 6 shows the EDM machining scene, and Fig. 7 shows the crater texture measurement scene. Fig. 8 and Fig. 9 show the image layer of the crater texture and the deep diameter curve of the crater texture, respectively. The depth of a single crater was 130 μm.

5 Analysis of cutting results of GCr15 hardened steel based on surface texture

5.1 Analysis of cutting force results

From the comprehensive cutting simulation and experimental data, it can be concluded that ap=300 μm, v=8500 mm/min, and f=100 μm/r was the best combination of parameters for this cutting experiment. The minimum cutting force obtained under this best parameter combination was 71.48 N. The CBN tool was selected to perform hard-state cutting on the workpiece with preset surface weaving under the optimal combination of cutting parameters. The cutting force curve shown in Fig. 10 was obtained by using a Kistler force measuring instrument. The cutting force data was then processed. The average cutting force for the hard-cutting experiment with the preset surface texture was 44.64 N, which was 26.84 N less than that without texture, a reduction of approximately 37.55%.

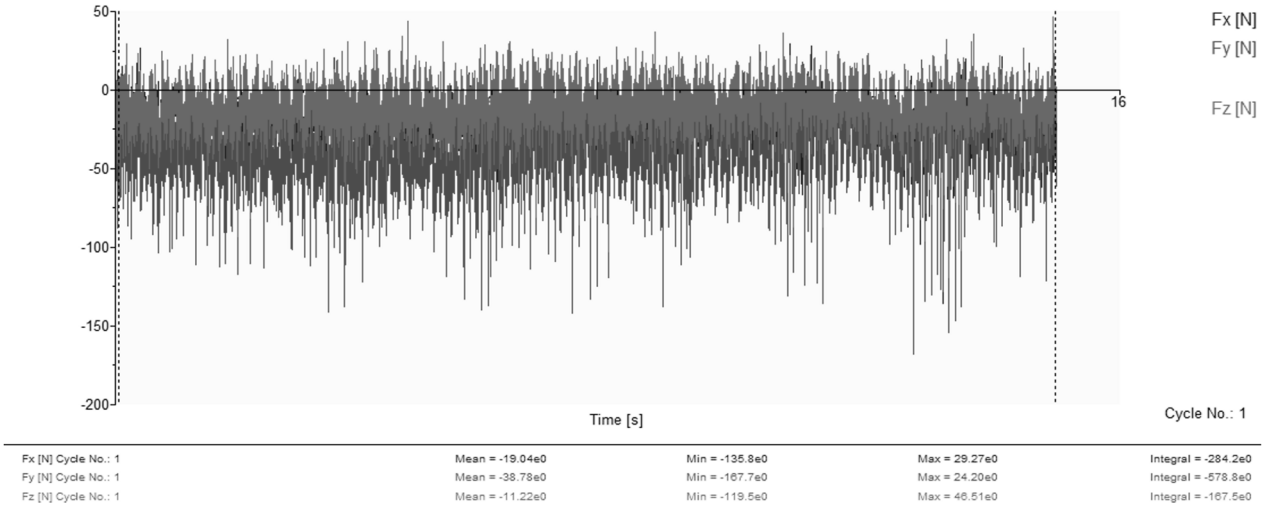

Fig. 10 *Cutting force curve of preset surface texture*

5.2 Analysis of tool wear results

The same type of tool was used to perform the same quantitative cutting process on the workpiece, with and without the preset texture. The tool numbers were denoted as a and b, and the front and rear tool faces were observed. Figures 11–18 show the observation results of the front and rear tool faces.

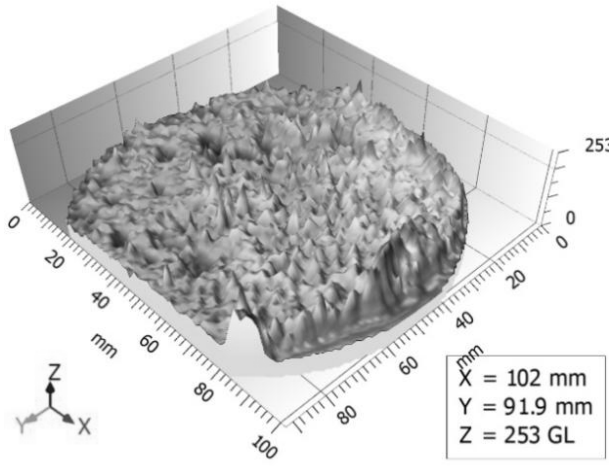

Fig. 11 *3D morphology of the rake face of knife a*

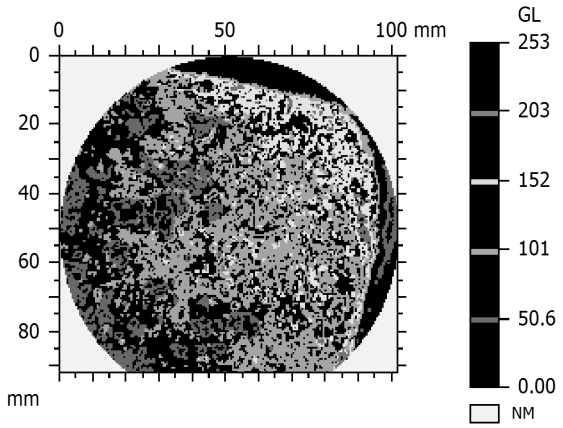

Fig. 12 *Contour lines of rake face of knife a*

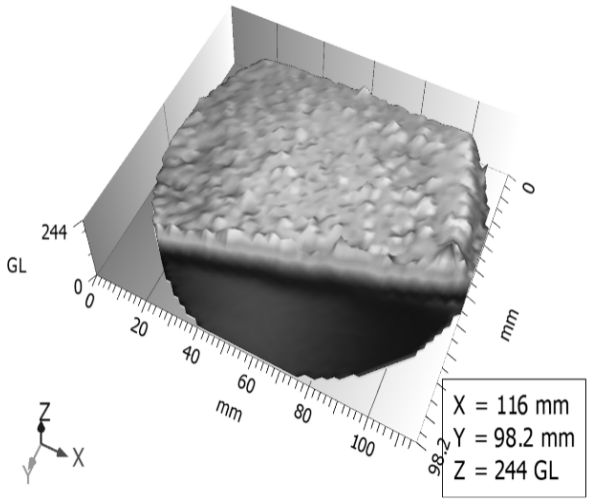

Fig. 13 *3D topography of the flank face of knife a*

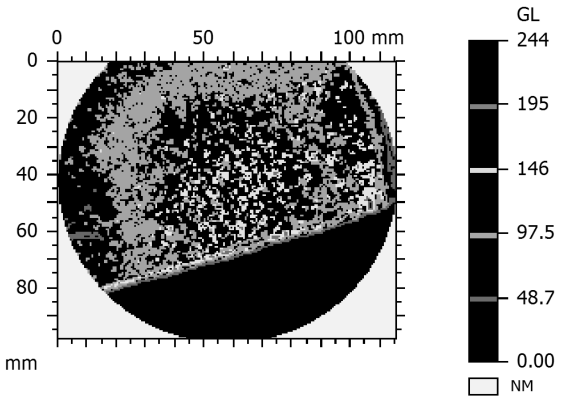

Fig. 14 *Contour lines of flank face of knife a*

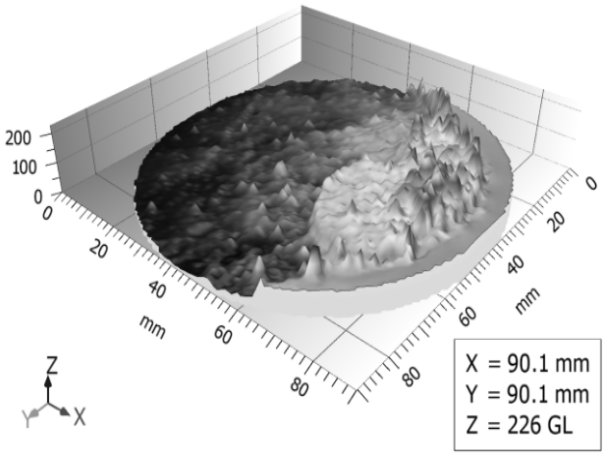

Fig. 15 *3D morphology of the rake face of knife b*

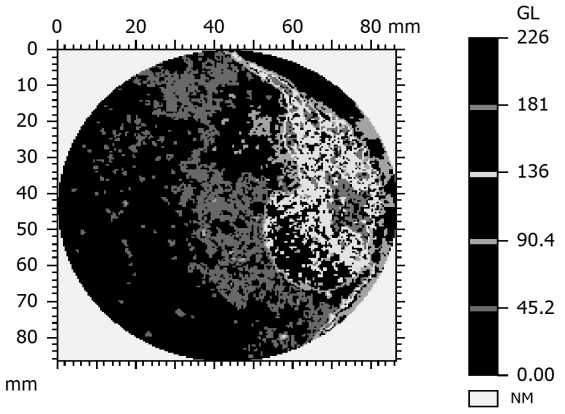

Fig. 16 *Contour lines of rake face of knife b*

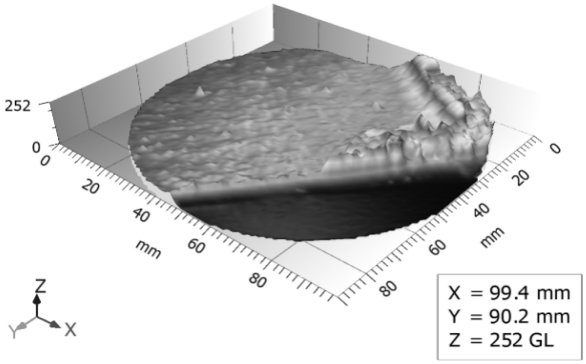

Fig. 17 *3D topography of the flank face of knife b*

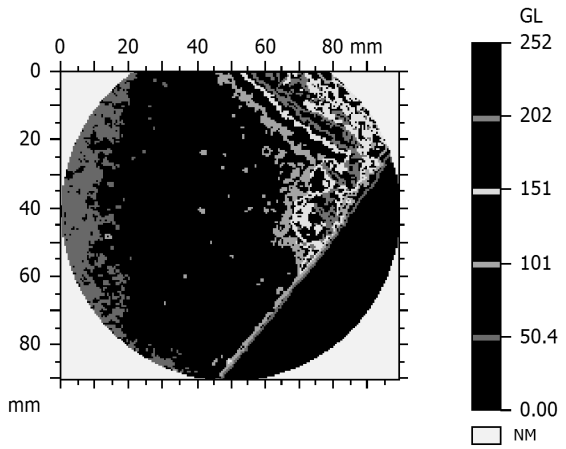

Fig. 18 *Contour lines of flank face of knife b*

When the front and rear face wear of tools a and b were compared and analyzed (Figs. 11, 15 and Figs. 13, 17), the front and rear face wear areas of tool a were large, and the wear position was irregularly distributed. The front and rear face wear areas of tool b were small, and the wear position was concentrated near the edge. As can be seen from Figs. 12, 16 and Figs. 14, 17, the front face contour maximum of tool a was 203 nm. The maximum height of the contour of the front face of tool a was 203 nm, and the maximum height of the rear face was 195 nm. The maximum height of the contour of tool b was 181 nm, and the maximum height of the rear face was 202 nm. The wear amount and wear area of the front and rear faces of tool b were smaller than those of tool a, and although the value of the contour of the rear face of tool b was larger than that of tool a, the difference between them was smaller.

In summary, since CBN tools are super hard, with hardness ranging from 7300–9000 HV, the cutting force generated during hard cutting is too large, which aggravates tool wear. Due to the tool's poor heat dissipation ability, leading to high tool temperature and tool oxidation at high temperature and pressure, the form of wear is bonded diffusion wear. From the previous analysis, it can be seen that the preset surface texture can effectively inhibit the generation of a large cutting force. Since the preset texture causes the chip layer to become thinner and more conducive to heat dissipation, it reduces the temperature of the tool during cutting, thereby reducing tool wear.

6 Conclusion

In this study, cutting simulation and hard-state cutting experiments were combined to determine the factors having the greatest degree of influence on cutting forces by the controlled variable method. The optimal combination of cutting parameters was derived by comparing the simulated cutting force data with the experimental cutting force data. Under the optimal combination of cutting parameters, the cutting force data with and without texture were compared and the tool wear before and after was analyzed. The following main conclusions can be drawn.

- For GCr15 bearing steel and hard cutting, the cutting force generated by the tool during hard cutting was measured, and the cutting simulation and experimental data were compared. Multiple analysis methods were combined to jointly determine ap=300 μm, v=8500 mm/min, and f=100 μm/r as the best combination of cutting parameters. The relationship between the degree of influence of the three factors on the most cutting force is as follows: $v < f < ap$. The minimum value of cutting force obtained under this optimal combination of parameters was 71.48 N
- The minimum cutting force of 44.64 N obtained with the optimal combination of cutting parameters for the workpiece surface preset texture performed using the EDM technique was approximately 37.55% lower than the minimum cutting force of 71.48 N obtained from the no-texture cutting experiment
- By observing the wear on the front and rear tool faces of the workpieces, with and without preset texture, in the same quantitative cutting process, it can be concluded that the machining method with preset surface texture can effectively reduce the tool wear

In this study, we combined surface weaving technology with hard-state cutting. The results indicate that pre-positioning weaving on the workpiece surface can effectively reduce the cutting forces generated during hard-state cutting, thereby reducing tool wear and improving tool life. The proposed method can provide a new direction and inform future hard-state cutting experiments.

Reference

[1] QIU CAIYUN (2009). Discussion on Cutting Technology of Hardened Steel Materials Discussion on Cutting Technology of Hardened Steel Materials. *Modern trade industry*,21(19), pp.310-311

[2] RAMANUJ KUMAR, ASHOK KUMAR SAHOO, PURNA CHANDRA MISHRA, AMLANA PANDA, RABIN KUMAR DAS, SOUMIKH ROY (2019). Prediction of Machining Performances in Hardened AISI D2 Steel. *Materials Today: Proceedings*,18(Pt 7)

[3] WU ZAIXIN, WANG YAXIANG (2020). Parameter Optimization of 50HRC Hardened Steel for PCBN Tool Dry Finishing Car. *Computer Simulation*,37(06), pp. 181-186

[4] ALES JAROS, JOSEF SEDLAK, PETR JASEK (2019). The Investigation of the Influence of Modern Coating Applied to the Cutting Inserts During Machining. *Manufacturing Technology*, 19(4), pp. 589-595

[5] SIGIT YOEWONO MARTOWIBOWO, BIVYNKA KEMALA DAMANIK (2021). Optimization of Material Removal Rate and Surface Roughness of AISI 316L under Dry Turning Process using Genetic Algorithm. *Manufacturing Technology*, 21(3), pp. 373-380

[6] TIPPANA SAHACHAR REDDY, TANMOY BANIK, RAMYA VELAGALA, SATADRU KASHYAP (2020). A study and modeling of cutting forces in dry turning of heat treated AISI H13 tool steel with brazed tungsten carbide tip. *Elsevier Ltd*, 24(Pt 2)

[7] Y. KEVIN CHOU, CHRIS J EVANS, MOSHE M BARASH (2002). Experimental investigation on CBN turning of hardened AISI 52100 steel. *Elsevier B. V.*, 124(3)

[8] JÁNOS KUNDRÁK, ZOLTÁN PÁLMAI (2019). The Change of Tool Life in a Wide Range of Cutting Speeds in Hard Turning. *Manufacturing Technology*, 19(2), pp. 254-260

[9] DENIS BOING, LEONARDO ZILLI, CARLOS ERNANI FRIES, ROLF BERTRAND SCHROETER (2019). Tool wear rate of the PCBN, mixed ceramic, and coated cemented carbide in the hard turning of the AISI 52100 steel. *Springer London*, 104(9-12)

[10] SILVIA SLABEJOVÁ, JOZEF HOLUBJAK, PAVOL TIMKO (2022). Cutting Forces in the Milling of Difficult-to-Machine Material used in the Aero Space Industry Using a Monolithic Ceramic Milling Cutter. *Manufacturing Technology*, 22(2), pp. 211-217

[11] BAI WEI (2018). Experimental Research on Vibration-assisted Cutting Mechanism and Machinability of Typical Difficult-to-machine Materials. Huazhong University of Science and Technology

[12] WU DEBAO (2019). Simulation analysis and experimental study of axially ultrasonic vibration turning. Shandong University

[13] DU QIANG (2018). Laser-assisted high-speed precision micro cutting device design and experimental research. Changchun University of Technology

[14] XU JINKAI, DU QIANG, WANG ZHICHAO (2018). Laser-assisted high-speed turning of nickel-based alloy GH4169 surface quality study. *Aerospace precision manufacturing technology*, 54(02), pp. 1-5

[15] DENIS BOING, LEONARDO ZILLI, CARLOS ERNANI FRIES, ROLF BERTRAND SCHROETER (2019). Tool wear rate of the PCBN, mixed ceramic, and coated cemented carbide in the hard turning of the AISI 52100 steel. *Springer London*, 104(9-12)

[16] ZHOU BAIJIAN, NIU QIULIN, LI PENGNAN, QIU XINYI (2019). Research status and progress of ultrasonic vibration assisted cutting of SiCp/Al composites. *Tool technology*, 53(09), pp. 3-8

[17] BO ZHANWEI (2016). Key technologies and scientific issues in laser heating assisted cutting. *Science Technology and Engineering*, 16(21), pp. 140-149

[18] LI ZHU, ZHANG QINGYONG, KONG LINGHUA, LIAN GUOFU, YANG JINWEI (2022). Characterization of hardness for GCr15 steel based on laser-induced breakdown spectroscopy. *Heat Treatment of Metals*, 47(01), pp. 284-290

[19] MU YONGZHE, HE TIANTIAN, SHAO RUONAN, et al (2021). Effect of quenching holding time on microstructure and friction and wear properties of CCr15 bearing steel. *Transactions of Materials and Heat Treatment*,42(12), pp. 109-116

[20] HANQIANG WU, LIANG JIANG, XIA ZHONG, JINWEI LIU, NA QIN, LINMAO QIAN (2021). Exploring the role of -NH_2 functional groups of ethylenediamine in chemical mechanical polishing of GCr15 bearing steel. *Friction*,9(06), pp. 1673-1687

[21] YU XIANTAO, ZHANG HAORAN, TU MENGYING, et al (2018). Heat treatment process and equipment for bearing rings. *Heat Treatment of Metals*, 43, (10), pp. 86-89

[22] TAO LIANG, CHEN HAIHONG, CHEN CHAO, LIU AIJUN (2018). Research on Residual Stress of Bearing Steel Hard Cutting Surface. *Tool technology*, 52(12), pp. 80-83

[23] LI CHENWEI, LUO HUI, et al (2021). An Automatic Estimation Method for Signal-to-Noise Ratio of Magnetic Resonance Equipment. *China Medical Devices*,36(11), pp. 24-26+31

[24] D. PHILIP SELVARAJ, P. CHANDRAMOHAN, M. MOHANRAJ (2014). Optimization of surface roughness, cutting force and tool wear of nitrogen alloyed duplex stainless steel in a dry turning process using Taguchi method. Measurement, 49

[25] WANG TING (2016). Hard aluminum alloy cutting and hardening law based on orthogonal test. *Light Metals*, pp. 47-48

[26] H. RAMAKRISHNAN, R. BALASUNDARAM, P. SELVAGANAPATHY, M. SANTHAKUMARI, P. SIVASANKARAN, P. VIGNESH (2019). Experimental investigation of turning Al 7075 using Al2 O3 nano-cutting fluid: ANOVA and TOPSIS approach. *SN Applied Sciences*, 1(12)

[27] LIU LIANGBAO, SUN JIANFEI, CHEN WUYI, WANG WEI (2015). Research on Turning Force of 27SiMn Steel Based on Orthogonal Test Method. *Journal of Hebei University of Science and Technology*, 36(06), pp. 553-558

[28] WANG XIAO, ZHU HONGBO (2015). Finite Element Simulation Research on 25CrMo Steel Cutting Force Based on Orthogonal Experiment. *Electromechanical Technology*, pp. 113-116

[29] VIET D. BUI, JAMES W. MWANGI, ANN-KATHRIN MEINSHAUSEN, ANDREAS J. MUELLER, JESSICA BERTRAND, ANDREAS SCHUBERT (2020). Antibacterial coating of Ti-6Al-4V surfaces using silver nano-powder mixed electrical discharge machining. *Surface & Coatings Technology*, 383